GPS Solutions (2023) 27:43
https://doi.org/10.1007/s10291-022-01381-6

ORIGINAL ARTICLE

# Evaluation of real-time variometric approach and real-time precise point positioning in monitoring dynamic displacement based on high-rate (20 Hz) GPS Observations

**Mert Bezcioglu[1] · Cemal Ozer Yigit[1] · Baris Karadeniz[1] · Ahmet Anil Dindar[2] · Ahmed El-Mowafy[3] · Özgür Avci[4]**

Received: 9 February 2022 / Accepted: 9 December 2022 / Published online: 22 December 2022


## Abstract

We present the performance of real-time (RT)-precise point positioning (PPP) and GNSS-based variometric approach for displacement analysis stand-alone engine (VADASE) methods in capturing dynamic motions in real time. To examine the effectiveness of the two RT methods, different cases, including harmonic motions in various frequency and amplitude ranges, two ground motions similar to those experienced during a real earthquake, and step motions, were generated using a shake table. RT-PPP and VADASE results based on global positioning systems (GPS) observations at a 20 Hz sampling rate were compared with results of the linear variable differential transformer (LVDT) sensor and relative positioning (RP) in the frequency and time domains. Frequency-domain outcomes demonstrated that both RT-based techniques can precisely detect dominant frequencies of the tested motions. However, the time domain results showed that the VADASE can capture the dynamic displacements slightly better than the RT-PPP. While the RMSE values of the differences between the RT-PPP technique and the LVDT vary between 2.3 and 11.6 mm, these values ranged from 1.4 to 6.00 mm for the VADASE approach. Results of earthquake simulation and step motion tests indicated that the VADASE provides more accurate and reliable results than the RT-PPP. It was concluded that the RT-PPP and VADASE approaches can significantly contribute to real-time determination of accurate displacement and natural frequencies of engineering structures and seismic waveforms. They have potential benefits for structural health monitoring, earthquake/tsunami early warning systems, and rapid risk assessment applications.

**Keywords** Real-time variometric approach · RT-PPP · High-rate GPS · Dynamic displacement · Wave motions · Shake table

## Introduction

High-rate GPS positioning has emerged as a powerful tool for monitoring strong ground motions during earthquakes (Larson et al. 2003), tsunami early warning systems (Geng et al. 2013), rapid hazard assessment (Yigit et al. 2020) and structural health monitoring (Shen et al. 2019). RP and PPP have been widely used approaches for detecting seismic waves caused by strong ground motions and natural frequencies of engineering structures (Malys and Jensen 1990; Bock et al. 2000). For the RP technique, at least one fixed reference station is required, but during mega earthquakes, the estimated displacements from receiver stations are affected by vibration and displacements at the fixed station site (Shu et al. 2017). Some studies have demonstrated the usability of

✉ Cemal Ozer Yigit
cyigit@gtu.edu.tr

1 Department of Geomatics Engineering, Gebze Technical University, Gebze, Turkey

2 Department of Civil Engineering, Gebze Technical University, Gebze, Turkey

3 School of Earth and Planetary Sciences, Curtin University, Perth, Australia

4 Department of Continuous Monitoring and Reference Station Systems, Sistem A.Ş, Istanbul, Turkey

the high-rate PPP technique in structural health monitoring (Yigit et al. 2021) and GNSS-seismology (Xu et al. 2021).

International GNSS Service (IGS) provides three types of precise orbit and clock products; ultra-rapid, rapid, and final, which enable PPP solutions (Kouba 2015). At present, GNSS precise products have some latencies ranging from 17 to 41 h for rapid products to 12–18 days for the final products, which is not suitable for real-time applications. While ultra-rapid products with approximately 2 h of latency are available for near-real-time applications, they are useless for high-precision PPP applications due to their low accuracy (Wang et al. 2018). In addition, the IGS has provided real-time (RT) products, only for GPS, through Networked Transport of RTCM via Internet Protocol (NTRIP) with an accuracy of 0.3 ns for the clock and 5 cm for orbit information (Hadas and Bosy 2015). Moreover, some studies tested the accuracy of RT products in both kinematic (Wang et al. 2019; Nie et al. 2020) and static modes (Elsobeiey and Al-Harbi 2016). RT-PPP is becoming an essential technique for earthquake and tsunami early warning systems (Melgar et al. 2020) and structural health monitoring studies (Tu et al. 2017). Capilla et al. (2016) investigated the usability of the RT-PPP technique in deformation monitoring with observations at 1 Hz sampling rate, and they concluded that the method can detect deformations up to 5 cm with an accuracy of $\pm 2$ cm. Tang et al. (2017) evaluated the performance of the RT-PPP technique in bridge monitoring with GNSS data at a 10 and 20 Hz sampling rate, and they suggested that the RT-PPP could be an alternative to the RP approach. Moreover, some studies evaluated the ability of the high-rate PPP technique for detecting co-seismic deformations under real-time conditions (Li et al. 2019; Zheng et al. 2019).

Real-Time Service (RTS) products, however, have limitations. RT-PPP applications are severely affected when communication with the user is poor and/or RTS data cannot be received (Nie et al. 2018). VADASE technique proposed by Colosimo et al. (2011), on the other hand, can determine the velocity of the GPS receiver by using the broadcast ephemeris; hence, unlike the RT-PPP technique, it does not require any internet connection. VADASE approach provides velocity or displacement information in real-time for users. Some studies investigated the kinematic applications of the VADASE approach for the detection of co-seismic deformations. For example, Benedetti et al. (2014) compared the performance of the broadcast orbit-based VADASE approach in capturing strong ground motions with RP and PPP techniques and demonstrated that the VADASE approach can estimate dynamic displacement at cm order in both horizontal and vertical components. Geng et al. (2016) investigated the performance of the VADASE to detect real-time seismic waves using GPS and GPS + BeiDou observations at 1–5 Hz sampling rate, showing improved results by using the latter. Shu et al. (2018a) evaluated the ability of the VADASE to estimate displacements employing the 50 Hz single-frequency GPS data. They demonstrated that the VADASE can estimate seismic waveforms at cm level accuracy in all components, compared to post-processed PPP. Benedetti et al. (2017) demonstrated the benefit of integrating VADASE-based low-cost GNSS and MEMS accelerometer technology in obtaining more accurate displacement estimates. Shu et al. (2018b) introduced a method, which is relied on the integration of the velocity and displacement information derived from the acceleration data at the 200 Hz sampling rate, and the velocity and displacement values at the 1 Hz sampling rate obtained using the VADASE. They revealed that this approach can provide more precise velocities and displacements. Moreover, the performance of the VADASE approach for structural health monitoring applications has also been investigated. Benedetti et al. (2016) examined the performance of the VADASE to estimation of the small-amplitude oscillation motion with uBlox GPS receiver at 5 Hz sampling rate using a single-axis shake table. They reported that the U-Blox GPS receiver was restricted to a low rate, which is resulted in aliasing and a considerable underestimate of the oscillation amplitude, although the findings were promising for structural health monitoring studies. Fortunato et al. (2019) collected data at a 1 Hz sampling rate with an android-based smartphone, and detection of dynamic movements was evaluated with VADASE. Results showed that the VADASE method can detect low-frequency motions. Most recently, Bezcioglu et al. (2022) investigated the performance of single-frequency VADASE technique for structural health monitoring applications employing GPS and GPS + Galileo observations at 20 Hz sampling rate, and they showed that the use of GPS + Galileo improved displacement estimation compared to GPS-only solutions.

In the above-mentioned studies, RT-PPP and VADASE methods were not considered in real-time, but as a possible real-time scenario applied in a post-processing mode. In addition, both methods were investigated independently from each other and generally using 1 Hz GPS observations. Unlike previous studies, for the first time, we discussed the usability and effectiveness of both RT-PPP and VADASE methods based on 20 Hz GPS observations in terms of capturing dynamic motions and permanent displacements in real time. Three different types of experiments, namely harmonic motions, earthquake simulations, and step motions, were carried out using a single-axis shake table. In the harmonic motions test, sinusoidal dynamic movements were generated in the range of 0.25 to 8.0 Hz frequency and 5 to 10 mm amplitude. In the earthquake simulation testing, ground wave motions of selected sites from 1989 Loma Prieta and 1940 El-Centro

earthquakes were generated on the shake table to evaluate the real-time performances of the RT-PPP and VADASE techniques in early warning systems. In addition to these two experiments, step motion experiments were carried out to detect permanent displacements. To study and compare the performance of the methods, their results were compared with displacements measured by the LVDT sensor, which is used as a ground truth.

## Stand-alone GNSS receiver approaches for real-time solution

Displacements of a dynamic station can be estimated directly in real time by RT-PPP and VADASE techniques using the observations of a single GNSS receiver. While real-time orbit and clock corrections are required to obtain dynamic displacements in the RT-PPP technique, the VADASE approach relies only on GNSS broadcast ephemeris. In the following sections, the RT-PPP and VADASE approaches are described. Moreover, it is worth mentioning that while the RT-PPP technique generally works with dual-frequency GNSS observations, the VADASE approach can work with both single and dual-frequency data.

### Real-Time PPP

In RT-PPP, raw code and phase observations are used. Their equations are expressed as:

$$P_{\mathrm{r}}^{s}(t_{\mathrm{r}}) = \rho_{\mathrm{r}}^{s}(t^{s}) + c\left(\delta t_{\mathrm{r}} - \delta t^{s}\right) + T_{\mathrm{r}}^{s}(t_{\mathrm{r}}) + I_{\mathrm{r}}^{s}(t_{\mathrm{r}}) + m\_p_{\mathrm{r}}^{s}(t_{\mathrm{r}}) + \varepsilon_{\mathrm{r,P}}^{s} \tag{1}$$

$$\begin{aligned}\phi_{\mathrm{r}}^{s}(t_{\mathrm{r}}) =& \rho_{\mathrm{r}}^{s}(t^{s}) + \lambda N_{\mathrm{r}}^{s} + c\left(\delta t_{\mathrm{r}} - \delta t^{s}\right) + T_{\mathrm{r}}^{s}(t_{\mathrm{r}}) \\ & - I_{\mathrm{r}}^{s}(t_{\mathrm{r}}) + m\_\phi_{\mathrm{r}}^{s}(t_{\mathrm{r}}) + \varepsilon_{\mathrm{r,L}}^{s}\end{aligned} \tag{2}$$

where $r$ and $s$ denote the receiver and satellite, and$P$ and $\phi$ are the GPS pseudorange (code) and carrier-phase measurement in meters, respectively. $t^{s}$ and $t_{\mathrm{r}}$ are the satellite and receiver signal times. $\rho$ describes the true geometric distance in meters between the antenna phase center of the satellite at transmission time and the antenna phase center of the receiver at reception time. $\delta t^{s}$ and $\delta t_{\mathrm{r}}$ specify the clock offsets for the satellite and receiver, respectively. $\varepsilon_{\mathrm{r,P}}^{s}$ and $\varepsilon_{\mathrm{r},\phi}^{s}$ present unmodeled errors and relevant system noise in meters for phase and code, respectively. $N$ and $\lambda$ are the integer ambiguity parameters in cycles and the wavelengths of the carrier phase for the thought frequency in meters, respectively. $c$ is the speed of light in vacuum. $I$ and $T$ are ionospheric and tropospheric components in meters.$m\_p_{\mathrm{r}}^{\mathrm{s}}$ and $m\_\phi_{\mathrm{r}}^{\mathrm{s}}$ are the multipath components for code and phase observations (Cai and Gao 2007).

IGS's real-time data streams present corrections of orbits and clocks with respect to broadcast ephemeris. Orbital corrections are presented in the radial ($\delta_{\mathrm{r}}$), along-track ($\delta_{\mathrm{a}}$) and cross-track ($\delta_{\mathrm{c}}$) directions with their velocities ($\delta_{\dot{r}}, \delta_{\dot{a}}, \delta_{\dot{c}}$) in RTCM-SSR (State Space Representation) format at reference epoch ($t_0$), denoted here as $\Delta_{\mathrm{ssr}}$, and include the issue of data (IOD) number (El-Mowafy et al. 2017), where:

$$\Delta_{\mathrm{ssr}} = \left(t_0, \mathrm{IOD}\right) = \left(\delta_{\mathrm{r}}, \delta_{\mathrm{a}}, \delta_{\mathrm{c}}, \delta_{\dot{\mathrm{r}}}, \delta_{\dot{\mathrm{a}}}, \delta_{\dot{\mathrm{c}}}, c_0, c_1, c_2\right). \tag{3}$$

$c_0, c_1, c_2$ are the polynomial coefficients to calculate clock corrections. Thus, orbit corrections at epoch $t$ can be calculated as:

$$\delta = \begin{bmatrix} \delta R \\ \delta A \\ \delta C \end{bmatrix} = \begin{bmatrix} \delta_{\mathrm{r}} \\ \delta_{\mathrm{a}} \\ \delta_{\mathrm{c}} \end{bmatrix} + \begin{bmatrix} \delta_{\dot{\mathrm{r}}} \\ \delta_{\dot{\mathrm{a}}} \\ \delta_{\dot{\mathrm{c}}} \end{bmatrix}\left(t - t_0\right) \tag{4}$$

Since the corrections are provided in the satellite-fixed coordinate system, orbit corrections need to be converted to earth-centered earth-fixed (ECEF) frame using the unit vectors ($e_{\mathrm{A}}, e_{\mathrm{c}}, e_{\mathrm{r}}$) in the along-track, cross-track and radial directions.

$$e_{\mathrm{A}} = \frac{\dot{r}}{|\dot{r}|}, e_{\mathrm{c}} = \frac{r \times \dot{r}}{|r \times \dot{r}|}, e_{\mathrm{R}} = e_{\mathrm{A}} \times e_{\mathrm{c}} \tag{5}$$

where $r$ and $\dot{r}$ are the satellite position and velocity position vectors obtained from the broadcast ephemeris. The precise orbit position in real-time can be computed after transforming the corrections from the satellite-fixed system to the geocentric system.

$$\begin{bmatrix} X_{\mathrm{p}} \\ Y_{\mathrm{p}} \\ Z_{\mathrm{p}} \end{bmatrix} = \begin{bmatrix} X_{\mathrm{b}} \\ Y_{\mathrm{b}} \\ Z_{\mathrm{b}} \end{bmatrix} + \begin{bmatrix} e_{\mathrm{R}} & e_{\mathrm{A}} & e_{\mathrm{c}} \end{bmatrix} \begin{bmatrix} \delta R \\ \delta A \\ \delta C \end{bmatrix} \tag{6}$$

where subscripts $b$ and $p$ refer to broadcast and precise position, respectively.

To compute the precise clock information at the current epoch, polynomial coefficients $c_0, c_1, c_2$ are used;

$$\mathrm{d}T_{\mathrm{p}} = \mathrm{d}T_{\mathrm{b}} + \frac{c_0 + c_1\left(t - t_0\right) + C_2\left(t - t_0\right)^2}{c} \tag{7}$$

where $T_{\mathrm{p}}$ and $T_{\mathrm{b}}$ denote real-time precise and broadcast clock products, respectively.

### VADASE

A variometric approach to detect dynamic motions in real time was proposed by Colosimo et al. (2011). The functional model of this approach is based on the epoch difference ($\Delta$) of the raw carrier phase observations collected by a single receiver. By taking the difference of the raw code observations between two

consecutive epochs, and assuming that dual-frequency observations are available, it gives:

$$\left[\lambda\phi_{\mathrm{r}}^{s}\right]_{\mathrm{L1}}+\beta\left[\lambda\phi_{\mathrm{r}}^{s}\right]_{\mathrm{L2}}=(e_{\mathrm{r}}^{s}\cdot\xi_{\mathrm{r}}+c\delta t_{\mathrm{r}})+(\left[\rho_{\mathrm{r}}^{s}\right]_{OR}-c\delta t^{s}+T_{\mathrm{r}}^{s}+\left[\rho_{\mathrm{r}}^{s}\right]_{\mathrm{EtOl}}+p_{\mathrm{r}}^{s})+m\_\phi_{\mathrm{r}}^{s}+\varepsilon_{\mathrm{r}}^{s} \tag{8}$$

where $=\left(f_{\mathrm{L1}}^{2}/\left(f_{\mathrm{L1}}^{2}-f_{\mathrm{L2}}^{2}\right)\right)$ and $\beta=\left(-f_{\mathrm{L2}}^{2}/\left(f_{\mathrm{L1}}^{2}-f_{\mathrm{L2}}^{2}\right)\right)$ represent the standard coefficients of the $\phi$ 1 and ϕ 2 combination ($f$ is the signal frequency); Δ denotes the time (epoch) difference. $p_{\mathrm{r}}^{s}$ is the sum of the other error sources (e.g., relativistic effects, phase center variations, phase wind-up);$\Delta\varepsilon_{\mathrm{r}}^{s}$ and $\Delta m_{\mathrm{r}}^{s}$ and correspond to the temporal difference of noise and multipath effects for the combined two frequencies, respectively. $e_{\mathrm{r}}^{s}$ describes the unit vector between satellite and receiver at time t; $\Delta\xi_{\mathrm{r}}$ is the displacement of the receiver between two consecutive epochs and this value is equivalent to the mean velocity in this time interval. $\left[\rho_{\mathrm{r}}^{s}\right]_{OR}$ and $\left[\rho_{\mathrm{r}}^{s}\right]_{\mathrm{EtOl}}$ are the change of the geometric distance due to the Earth rotation and the satellite orbital motion, and the change of the geometric distance due to the ocean loading variations and solid Earth tides, respectively. $(e_{\mathrm{r}}^{s}\cdot\Delta\xi_{\mathrm{r}}+c\delta t_{\mathrm{r}})$ contains the 3D displacement ($\xi_{\mathrm{r}}$) and the receiver clock offset variation ($\delta t_r$). $\left(\left[\rho_{\mathrm{r}}^{s}\right]_{\mathrm{OR}}-c\delta t^{s}+T_{\mathrm{r}}^{s}+\left[\rho_{\mathrm{r}}^{s}\right]_{\mathrm{EtOl}}+p_{\mathrm{r}}^{s}\right)$ includes the known parameters that can be computed based on the chosen tropospheric model, broadcast orbit and clock models, and proper models for all of the considered effects.

With this approach, the velocities of the high-rate standalone receiver can be computed with order of mm $s^{-1}$ accuracy, and then, by integrating the computed velocities, estimated values are transformed to dynamic displacements (Li et al. 2014).

**Fig. 1** Shake table and three GNSS antennas mounted on the table. The yellow antenna is Leica CGA60, which collects the observations for VADASE solutions, while the beige antenna is Novatel GPS-702, which collects the observations for RT-PPP solutions. The gray/white antenna is CHC I80, employed for the RP solution. The LVDT sensor is embedded under the black plate of the shake table

## Experiment and data description

This section summarizes the use of real-time observations for dynamic motion monitoring. Figure 1 shows the shake table platform that was used in the experiment carried out in July 2021 at the Gebze Technical University, Turkey. The shake table has a 190-mm total stroke and motions controlled by computer software. During the tests, three GNSS antennas and an LVDT sensor were mounted on the table. One of these antennas, a Novatel GPS-702, was connected to Trimble MB-2 OEM receiver, which tracks only GPS observations and was employed for a real-time PPP solution, while the other antenna, Leica CGA60, was connected to a Leica GR30 receiver, which is capable of a real-time VADASE solution. The third antenna was the CHC I80 antenna/receiver assigned for the double-difference (DD) solution. Another CHC I80 antenna/receiver was installed at a known point approximately 70 m away from the shake table for DD processing. All GNSS receivers are set to a 20 Hz sampling rate and 10° elevation cutoff angle, and a LVDT sensor collects the data with a 100 Hz sampling rate. While the RTKNAVI module of RTKLIB software (Takasu and Yasuda 2009) was used for the real-time PPP solution, the Leica GR30 receiver recorded VADASE-derived displacements in real time. RTKPOST module of RTKLIB software was also used for the double differences (DD) solution. As mentioned before, the real-time precise clock and satellite corrections required in the RT-PPP solution were obtained from the IGC01 stream via products.igs-ip.net:2101. Three different forms of dynamic motions were generated in the experiments. These motions are harmonic oscillations, seismic ground wave motions, and step functions, respectively, and it took approximately half an hour to generate all these motions using the shake table.

Geocentric coordinates of the antennas in the ITRF system obtained from the RP and RT-PPP methods were converted to topocentric coordinate systems since the former system is not suitable for obtaining displacements along the movement direction of the shake table. As the VADASE method provides direct velocity and displacement in the east, north, and up directions, the coordinate transformation was not needed for its results. Finally, the dynamic displacements in the east and north direction, obtained from relative positioning, RT-PPP and VADASE, were projected into the movement direction of the shake table, as described in Yigit et al. (2021).

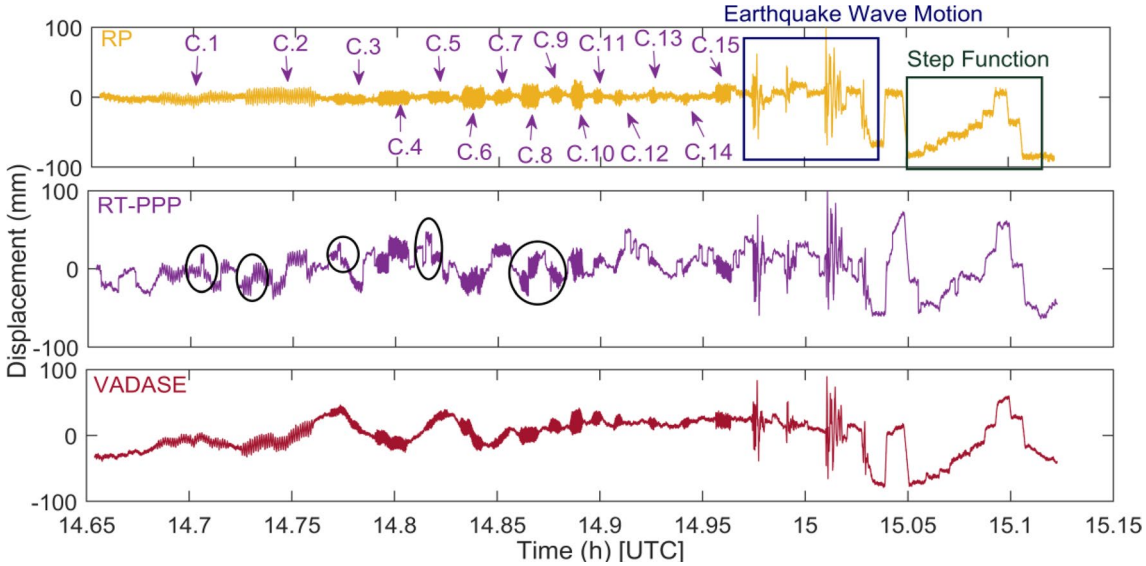


**Fig. 2** RP (top panel), RT-PPP (middle panel), and VADASE (bottom panel) derived displacements. Time series are detrended, and they contain all dynamic displacement experiments, namely harmonic motions, earthquake simulations, and step motions. While RT-PPP and VADASE solutions were obtained in real-time, RP solutions were evaluated in post-mission mode. C.# in the top panel denotes the Case number

## Results and discussion

This section evaluates the performance of the RT approaches for dynamic motion detection. For the three designed experiments, LVDT data were taken as a reference to evaluate the accuracy of the other methods. Since the LVDT has a 100 Hz sampling rate, it was down-sampled to 20 Hz to carry out this comparison.

Figure 2 shows the displacement time series, which are obtained from the three approaches, including all dynamic motions generated using the shake table. From top to bottom, the time series refers to RP, RT-PPP with float ambiguity resolution, and VADASE. It can be seen that the RP-derived displacements are very consistent, whereas the RT-PPP- and VADASE-derived displacements exhibit long-term fluctuations. However, RT-PPP-derived displacements have more fluctuations than that of VADASE. Such fluctuations can be readily filtered out by implementing a high-pass filter to extract harmonic motions for rapid risk assessment applications in the post-mission mode (Wang et al. 2016). However, one should note that implementing high-pass filtering is not suitable for earthquake source parameter estimation as it would cause a loss of earthquake-induced co-seismic displacement if exists and ground wave motion pattern. Nevertheless, we applied a high pass filter to the harmonic motion cases in the post-mission mode to investigate the applicability of RT-PPP and VADASE for the rapid detection of structural damage after an earthquake. In addition to fluctuations, the RT-PPP-derived time series includes some sudden shifts, which are denoted by black-colored ellipses in Fig. 2. Such sudden jumps can be detected and eliminated by, e.g., spatial filtering or leave-one-out cross-validation (Benedetti et al. 2017; Hung et al. 2017). However, they were left in the time series in the figure to show their presence. The results of different tests will be analyzed and discussed in the next section.

## Harmonic motions experiments

The performance of the two RT solutions in capturing harmonic motions is evaluated in this section. To filter out long-term fluctuations and to evaluate the usability of the two RT solutions for rapid risk assessment, a 5th-order high-pass Butterworth filter with a cutoff frequency of 0.20 Hz was used. For consistency of the comparisons, the same filter was applied to the RP-based displacement components. Figure 3 shows the filtered time series of all approaches. The frequency and amplitude of different harmonic oscillation cases generated using the shake table are summarized in Table 1. From Fig. 3, it seems that RP- and VADASE-derived displacements are very consistent, whereas RT-PPP-derived displacements have some spikes, which are marked by ellipses, due to sudden shifts in time series. This is most likely due to ambiguity re-initialization of a sudden change in the orbital and clock corrections.

Case 15 is a superimposed motion including multiple frequencies and amplitude values, which we will discuss here as a representative example to illustrate and compare the performance of all GPS-based methods in capturing dynamic

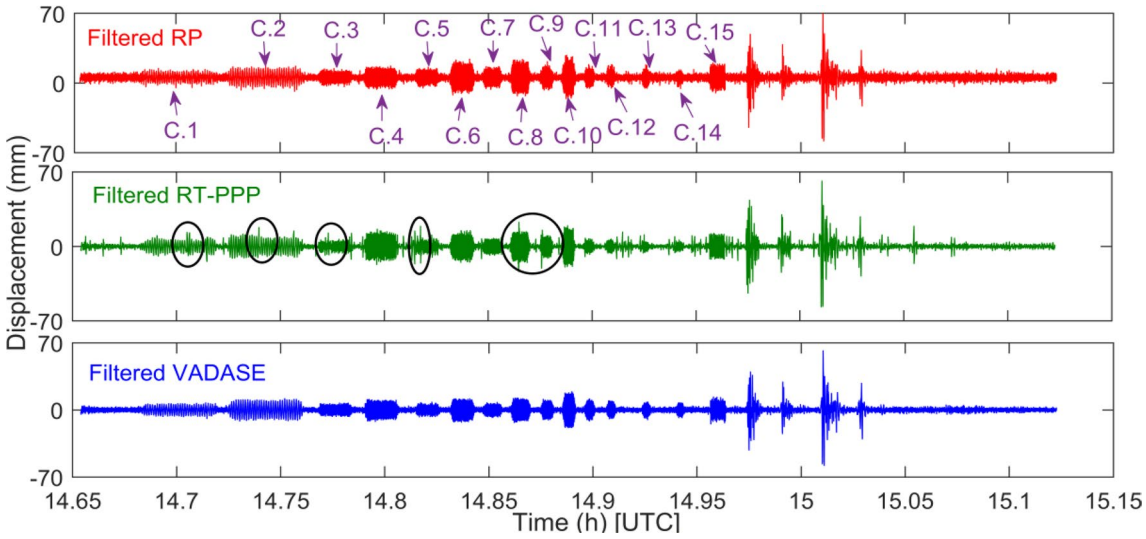


**Fig. 3** Filtered RP (top panel), filtered RT-PPP (middle panel), and filtered VADASE (bottom panel) derived displacements. Time series were filtered out using the 5th-order Butterworth high-pass filter with a cutoff frequency of 0.20 Hz. The filtering process was applied to harmonic motions

**Table 1** Frequency and amplitude values of each case generated using a single-axis shake in harmonic oscillation experiments. Case 15 is a superimposed motion that has multiple frequency values, while cases 1 to 14 have a single-frequency motion

| | Frequency (Hz) | Amplitude (mm) |
|---|---|---|
| Case 1 | 0.25 | 5 |
| Case 2 | 0.25 | 10 |
| Case 3 | 0.60 | 5 |
| Case 4 | 0.60 | 10 |
| Case 5 | 1.50 | 5 |
| Case 6 | 1.50 | 10 |
| Case 7 | 2.00 | 5 |
| Case 8 | 2.00 | 10 |
| Case 9 | 3.50 | 5 |
| Case 10 | 3.50 | 10 |
| Case 11 | 5.00 | 5 |
| Case 12 | 6.00 | 5 |
| Case 13 | 7.00 | 5 |
| Case 14 | 8.00 | 5 |
| Case 15 | 0.80 | 10 |
| | 3.40 | 5 |
| | 7.60 | 1 |

harmonic oscillations. Results of this case are shown in Fig. 4, which includes the LVDT-, RP-, RT-PPP-, and VADASE-derived displacement time series as well as their fast Fourier transform (FFT) spectrum. The figure shows that the displacements derived by RT-PPP and VADASE for both unfiltered and filtered time series are in good agreement with those derived by LVDT and RP. Furthermore, the results of the FFT spectrums of the reference LVDT and unfiltered and filtered GPS-based time series indicate that the detected peak frequency values are the same, whereas there are slight differences in the corresponding amplitudes. While the corresponding amplitude values for all three dominant frequencies did not change in the RP and VADASE techniques after filtering, the amplitude for the second dominant frequency obtained by RT-PPP changed by about 0.1 mm. Moreover, results of Case 1 to 14 are shown in Fig. S1–S14 in supplementary material.

FFT spectrum of the displacement time series for each event indicated in Table 1 was evaluated to further investigate the performance of the RT-PPP and VADASE methods, and the results are shown in table S1 in supplementary material. Values in brackets indicate the filtered results, whereas the other values are the unfiltered results. Oscillation frequencies obtained from the two sets of RT-based solutions for both filtered and unfiltered show good agreement with LVDT and RP, as shown in the table. However, there are slight differences in the corresponding amplitudes. The amplitude of oscillation frequency differences between LVDT and RT-PPP solutions ranges from 0.0 to 4.4 mm, whereas the amplitude of the oscillation frequency difference between RP and RT-PPP is between 0.0 and 3.3 mm. Differences between the VADASE method and the LVDT range between 0.1 and 5.2 mm, while the differences with the RP vary between 0.1 and 2.5 mm. This difference is mainly due to the use of different receiver and antenna types. In Table S1, it can be seen that the amplitude values obtained from VADASE are closer to the LVDT values than those obtained from the RT-PPP and RP estimated motions

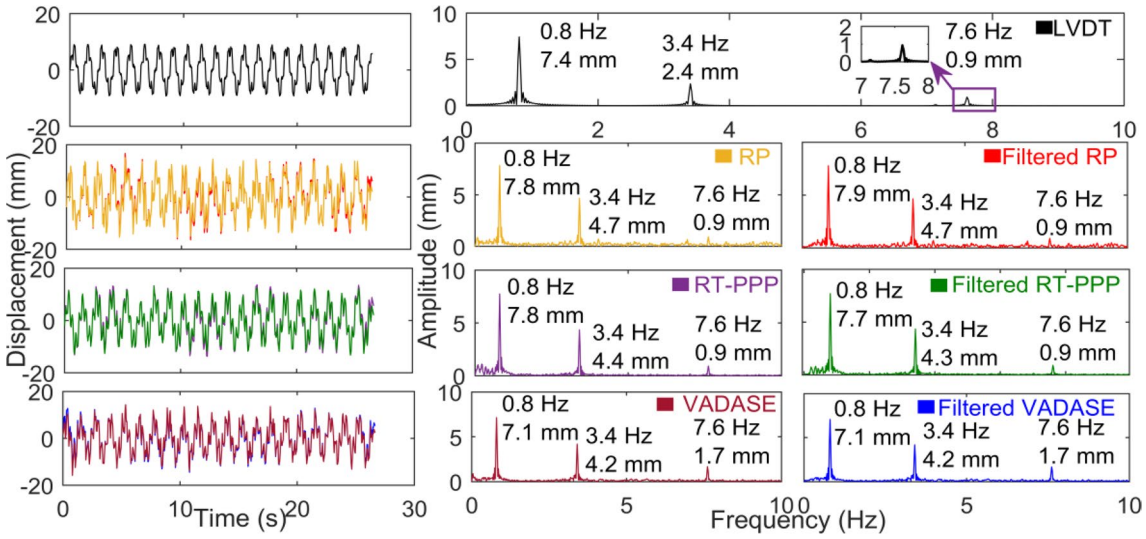


**Fig. 4** Displacement time series (left) and FFT spectrum (right) for (from top to bottom): LVDT, unfiltered and filtered RP, RT-PPP, and the VADASE approach, respectively, for case 15. While the filtered and unfiltered displacement time series of the GPS methods were plotted together in different colors, their FFT spectrums were plotted separately

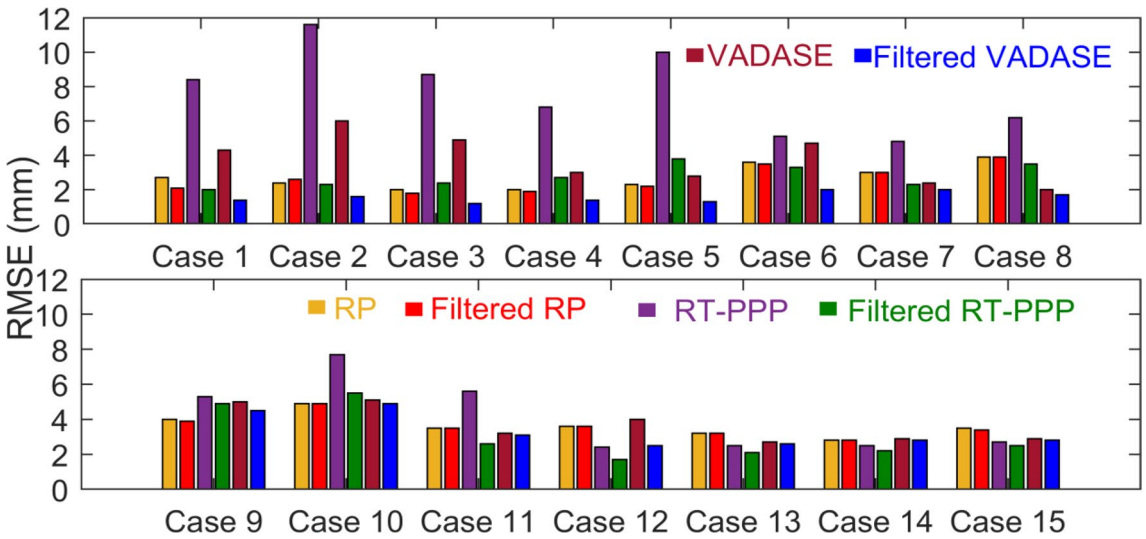


**Fig. 5** RMSE values of unfiltered and filtered RP, RT-PPP, and VADASE solutions for all designed harmonic motion experiments. RMSE values were derived from the differences between GPS-based methods and LVDT sensor for each case

and range between 0.25 and 2 Hz frequency. In oscillations with 3.5 Hz and higher frequency, RT-PPP and RP methods gave similar values that are closer to LVDT.

In addition to the frequency domain comparisons, the root mean square (RMSE) values of the displacement differences between the GPS-based approaches and the reference LVDT sensor were calculated to further investigate and compare the performance of these methods. Computed RMSE values are presented in Fig. 5. It can be seen that there are no significant differences between filtered and unfiltered RP solutions. For unfiltered RT-PPP solutions, high RMSE values stand out in low-frequency cases, especially for case 1 to case 5, which reaches up to 11.6 mm. However, as the motions of frequency increase, the RMSE values decrease. This can be explained by the fact that low-frequency cases take a longer time compared to high-frequency cases and are affected more than those cases by long-term fluctuations caused by residual errors due to limitations of error modeling capabilities, such as multipath, higher-order ionosphere and troposphere. RMSE values of the filtered RT-PPP solutions show good agreement with LVDT. After the filtering process, the RMSE values were reduced by between 7 and

80%. Although unfiltered VADASE shows similar behavior as unfiltered RT-PPP for both low and high-frequency cases, the unfiltered VADASE approach performs slightly better than the unfiltered RT-PPP technique. Similar to filtered RT-PPP, the RMSE values of filtered VADASE improved between 3 and 75%.

When focusing on the filtered results, it can be seen that the RMSE values of the RT-PPP and VADASE method are slightly better than that of the RP method in all cases except cases 3, 4, 5 and 9. This is mainly due to the amplification of noise by forming double-difference observations. Moreover, the VADASE method gives lower RMSE values than the RT-PPP method in the first 10 cases. On the contrary, RT-PPP has slightly lower RMSE values than other methods for cases 11 to 15. RMSE values obtained from the VADASE method are slightly smaller than RT-PPP at frequencies lower than 3.5 Hz, while the RMSE values obtained from the RT-PPP technique are slightly smaller than VADASE at frequencies higher than 5 Hz. Given that the RMSE differences between the methods are small, it does not mean that the VADASE approach captures oscillations up to 3.5 Hz significantly better than RT-PPP, or that RT-PPP captures oscillations above 5 Hz significantly better than VADASE. Therefore, further research and new experiments might be performed to confirm and clarify these findings. Furthermore, detailed statistical values of unfiltered and filtered RP, RT-PPP, and VADASE solutions for all harmonic motion experiments can be found in table S1 and S2 in supplementary material.

## Using RT-PPP and VADASE approaches for earthquake monitoring

This section evaluates the performance of the RT-PPP and VADASE approaches in detecting earthquake-induced ground wave motions for early warning systems. To do so, motions mimicking $M_w$ 6.9 of the Loma Prieta and $M_w$ 6.9 of the El Centro earthquakes were generated on the shake table. It is noteworthy that the earthquake early warning refers to the quick detection of earthquake-induced seismic waves and earthquake parameters such as the hypocenter location and the magnitude size and sending warnings to blind zone areas far from the earthquake epicenter, thus preventing secondary losses (Allen and Ziv 2011). GNSS-aided early warning system is important, especially for large earthquakes ($M < 7$) due to the fact that strong-motion accelerometers or broadband seismometers may not be operational beyond their limit values.

### $M_w$ 6.9 Loma Prieta of October 17, 1989

*M*W 6.9 Loma Prieta earthquake on the San Andreas fault line occurred on October 17, 1989. The earthquake was near to the surface, and its mechanism was a strike-slip. Even though the epicenter of the quake was in a rural area, the interstate highways were largely affected due to strong ground movements. Ground motion data used to simulate the Loma Prieta earthquake were recorded at Gilroy #1 station operated by the California Geological Survey (CGS). The recording station was approximately 30 km

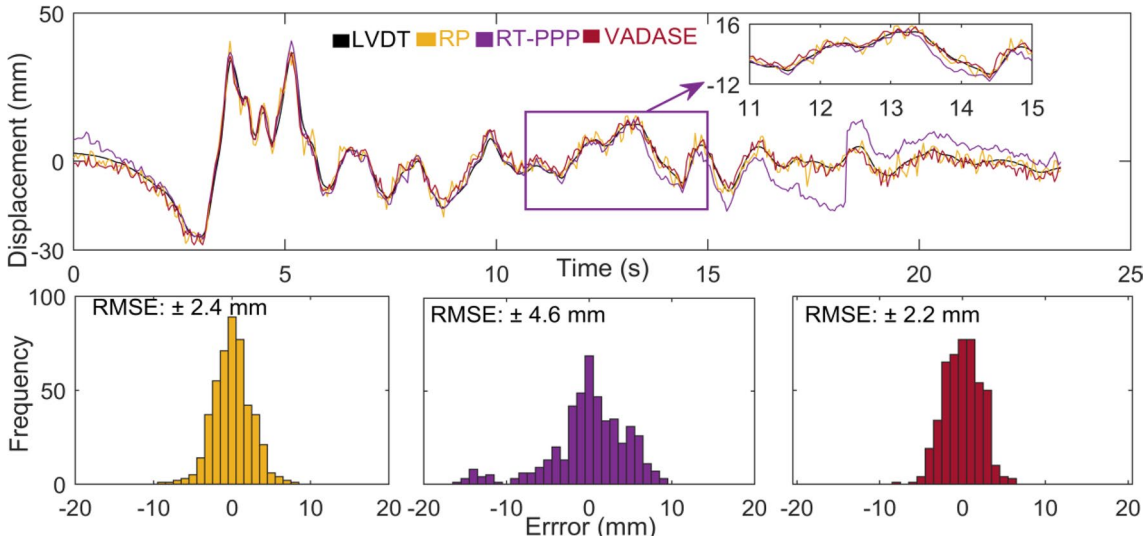


**Fig. 6** LVDT, RP, RT-PPP and VADASE-derived displacements during the 1989 $M_w$ 6.9 Loma Prieta Earthquake Simulation (top) and histograms of the differences between RP-, RT-PPP- and VADASE-derived displacements and LVDT (bottom). RMSE values were given in the histogram plots

from the epicenter and was free-field, resting on hard soil (VS30 = 1428 m/s). E-W component of the recorded data was used.

Figure 6 illustrates a time series of displacement generated by simulating the Loma Prieta earthquake record, as well as histograms of the differences between LVDT and GPS-based solutions. Time series derived from RP and VADASE are largely consistent with the reference LVDT sensor during the overall earthquake, while the RT-PPP-derived displacements are in good agreement with the LVDT during the first 14 s. However, after the 14th second, the waveforms were slightly separated from the LVDT sensor and there was a spike at a sudden shift at second 18. As a result of this sudden shift, the maximum difference between the waveforms obtained from the RT-PPP and LVDT sensors is 15.7 mm, and the RMSE is 4.6 mm. These results demonstrated that the RT-PPP technique is highly dependent on the real-time stream corrections. However, these sudden shifts can be easily detected and properly eliminated, but are shown here to demonstrate their presence when using RT-PPP. In the Loma Prieta earthquake test, the VADASE approach performed slightly better than the RP method. Maximum and RMSE values of the discrepancies from LVDT results are 9.2 and 2.4 mm for RP, 7.9 and 2.2 mm for VADASE, respectively. Considering these outcomes, it is clear that the VADASE approach can be a very powerful technique for early warning systems.

### $M_w$ 6.9 El Centro of May 19, 1940

May 18, 1940, Mw6.9 El Centro, the USA, was the first strong ground motion recorded by seismographs. Earthquake, which is a strike-slip type, occurred on San Andreas fault line and near the surface. Data used in the analysis were the *E-W* component of the ground motion recorded at Station 9 operated by the United States Geological Survey (USGS), which was used as a benchmark. Hypocentral distance of the station was 16 km.

Figure 7 illustrates the time series of displacement generated by simulating the El Centro earthquake's selected record and the histograms and RMSE values of the differences between the LVDT and GPS-based solutions. Displacement waveforms estimated from RP, RT-PPP, VADASE, and LVDT are considerably comparable in detecting dynamic ground motions. Displacement waveform differences between RP and LVDT are slightly greater than those between RT-based solutions and LVDT. The maximum value of the displacement differences between RP and LVDT is 13.1 mm, while the differences between RT-PPP/VADASE and LVDT range from − 10 mm to + 10 mm. The VADASE approach performed slightly better than the two methods. Unlike the Loma Prieta earthquake simulation, El-Centro earthquake simulation results show that the RT-PPP technique can precisely capture the simulated seismic ground waveforms.

## Overall discussion of the RT-PPP and VADASE approaches for earthquake monitoring

Results of the above two earthquake simulations showed that the VADASE approach is more accurate than the RT-PPP and even slightly better than RP. Differences between

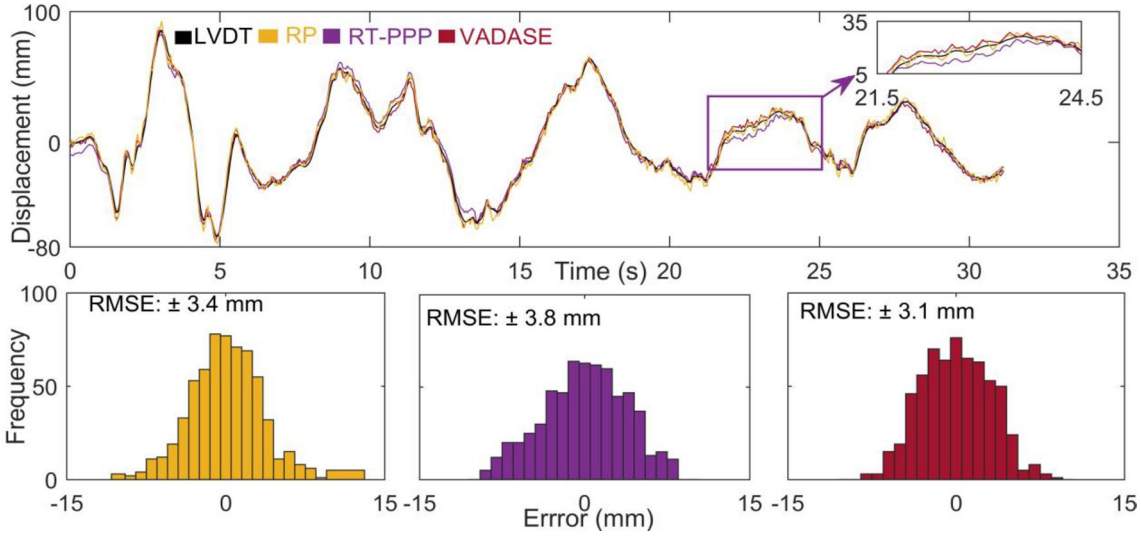


**Fig. 7** LVDT, RP, RT-PPP and VADASE-derived displacements during the 1940 $M_w$ 6.9 El Centro Earthquake Simulation (top) and histograms of the differences between RP-, RT-PPP- and VADASE-derived displacements and LVDT (bottom). RMSE values were given in the histogram plots

VADASE and LVDT were less than 8 mm for Loma Prieta earthquakes and less than 10 mm for the El Centro earthquake. As stated earlier, these findings clearly show that the VADASE technique can be a very powerful tool for detecting seismic waves. While the RT-PPP-derived waveform had some spikes in the Loma Prieto earthquake simulation, its performance was quite similar to RP and VADASE in the El Centro earthquakes. This performance difference is most likely due to the quality of the real-time orbit and clock corrections obtained from the IGC01 stream, which changes over time (Hadas and Bosy 2015; El-Mowafy et al. 2017). This indicates that the performance of the RT-PPP may experience some temporal variations, and as a result, it may not always achieve the desired level of accuracy. Overall, the outcomes of earthquake simulation experiments demonstrated that the VADASE approach can record seismic waveforms more precisely than the RT-PPP.

## Using RT-PPP and VADASE approaches for static or quasi-static displacement and deformation monitoring

To investigate the ability of the RT-PPP and VADASE method in terms of detecting quasi-static or permanent displacements, we performed a step motion experiment. In the experiment, 10 mm displacement was applied four times, and 20–50 mm displacements were generated, only once by the shake table, as shown in Fig. 8, which shows a comparison of step motions detected by the three approaches. One can observe that RT-PPP results had some long-term fluctuations. However, the RP result followed the displacements more accurately, and the VADASE-derived displacements are largely consistent with RP.

To further evaluate and compare the ability of the two RT methods, the permanent (static deformations) displacement values for each step motion were calculated and are summarized in Table S4 in supplementary material. Permanent displacement values were estimated by taking the difference of the averages of 200 consecutive epochs (10 s.) before and after generating step motion. Error propagation was applied to obtain the standard deviations of the estimated displacement. As expected, the RP technique almost accurately determined all displacement values. The maximum difference between the actual and RP-derived displacement was 3 mm for all experiments. However, the actual and RT-PPP-derived displacement difference ranged between 2 and 16 mm. Differences between the actual and VADASE-derived displacements were less than 13 mm. While the average difference for VADASE was 5.8 mm, it was 9.3 mm for the RT-PPP method. These results imply that RT-PPP and VADASE can be employed to detect real-time co-seismic displacement and rapidly assess strong/large earthquake mechanisms. Moreover, these results showed that the former method is slightly better than the latter method in terms of capturing quasi-static/permanent displacement in real time.

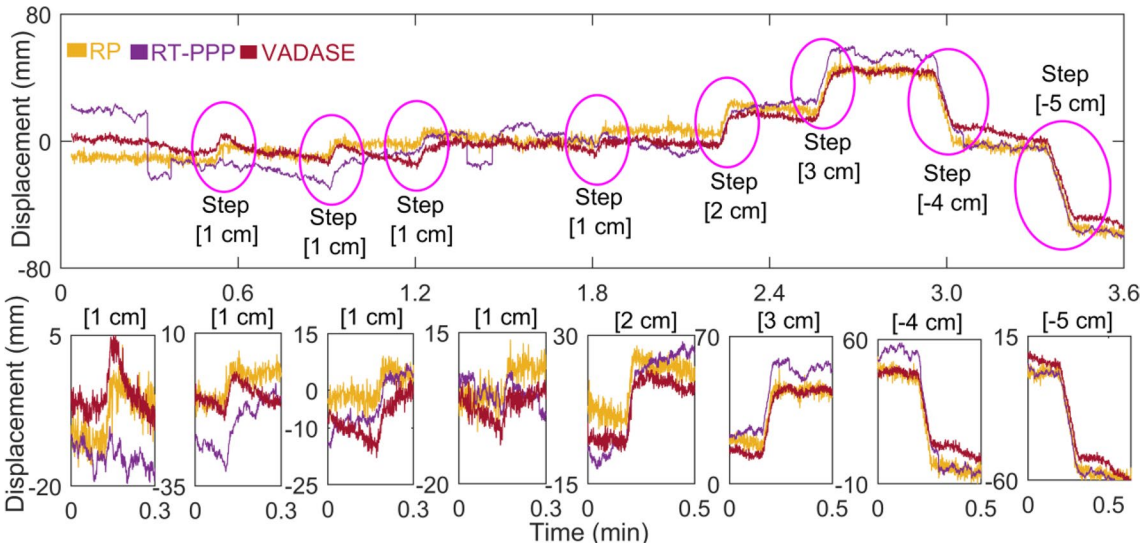


**Fig. 8** RP-, RT-PPP- and VADASE-derived displacements during the step motion experiments (top) and a detailed examination of the step motions detected by all discussed GPS methods, namely RP, RT-PPP and VADASE (bottom). In the step motion experiments, four 10 mm, and one 20, 30, 40 and 50 mm displacements were generated, respectively

## Conclusion

We present the performance of RT-PPP with RTS products and VADASE approaches to detect short-term dynamic motions, seismic waveforms, and permanent displacement. Analysis of the harmonic oscillation experiments in the frequency domain showed that frequencies up to 8.0 Hz can be successfully detected with both the RT-PPP and VADASE approaches. Findings in the time domain emphasized that the VADASE approach performed slightly better than the RT-PPP technique. In addition to the product and algorithm differences used, different antenna and receiver types used in the experiment may cause these small differences (Ebinuma and Kato 2012). Harmonic oscillation experiments demonstrated that structural health monitoring systems can be operated with RT-PPP or VADASE approaches. Results of earthquake simulations demonstrated that the VADASE method closely follows the LVDT in the two earthquake simulations and is even partially better than the RP method. This indicates that, at least in this research, the VADASE method is more reliable and accurate than the RT-PPP method. The step motion experiment showed that VADASE could detect permanent displacements slightly better than the RT-PPP method. Although RT-PPP might be easily used for near real-time applications, RT-PPP with RTS products could be employed in real-time applications providing those corrections are available and the delay is less than 1 s. Since the RT-PPP technique depends on real-time precise orbit and clock corrections streams via the internet, it might suffer from latency and interruptions of this service. In contrast, the VADASE approach uses the broadcast ephemeris to obtain velocity and displacement of motion. Thus, the VADASE approach may ensure continuous solutions for real-time applications.

**Supplementary Information** The online version contains supplementary material available at https://doi.org/10.1007/s10291-022-01381-6.

**Acknowledgments** Authors would like to thank Sistem A.Ş and Leica Geosystems for providing the Leica GR30 GNSS receiver and VADASE engine.

**Data availability** Data that support the findings of this study are available from the corresponding author upon reasonable request.

## References

Allen RM, Ziv A (2011) Application of real-time GPS to earthquake early warning. Geophys Res Lett 38:L16310. https://doi.org/10.1029/2011GL047947

Benedetti E, Branzanti M, Biagi L, Colosimo G, Mazzoni A, Crespi M (2014) Global navigation satellite systems seismology for the 2012 Mw 6.1 Emilia earthquake: exploiting the VADASE algorithm. Seismol Res Lett 85(3):649–656. https://doi.org/10.1785/0220130094

Benedetti E, Ravanelli R, Moroni M, Nascetti A, Crespi M (2016) Exploiting performance of different low-cost sensors for small amplitude oscillatory motion monitoring: preliminary comparisons in view of possible integration. J Sens 2016:7490870. https://doi.org/10.1155/2016/7490870

Benedetti E, Dermanis A, Crespi M (2017) On the feasibility to integrate low-cost MEMS accelerometers and GNSS receivers. Adv Sp Res 59(11):2764–2788. https://doi.org/10.1016/j.asr.2017.02.005

Bezcioglu M, Yigit CO, Mazzoni A, Fortunato M, Dindar AA, Karadeniz B (2022) High-rate (20 Hz) single-frequency GPS/GALILEO variometric approach for real-time structural health monitoring and rapid risk assessment. Adv Sp Res 70(5):1388–1405. https://doi.org/10.1016/j.asr.2022.05.074

Bock Y, Nikolaidis RM, De Jonge PJ, Bevis M (2000) Instantaneous geodetic positioning at medium distances with the global positioning system. J Geophys Res Solid Earth 105(B12):28223–28253. https://doi.org/10.1029/2000jb900268

Cai C, Gao Y (2007) Precise point positioning using combined GPS and GLONASS observations. J Glob Position Syst 6(1):13–22. https://doi.org/10.5081/jgps.6.1.13

Capilla RM, Berné JL, Martín A, Rodrigo R (2016) Simulation case study of deformations and landslides using real-time GNSS precise point positioning technique. Geomat Nat Hazards Risk 7(6):1856–1873. https://doi.org/10.1080/19475705.2015.1137243

Colosimo G, Crespi M, Mazzoni A (2011) Real-time GPS seismology with a stand-alone receiver: a preliminary feasibility demonstration. J Geophys Res Solid Earth 116(11):1–14. https://doi.org/10.1029/2010JB007941

Ebinuma T, Kato T (2012) Dynamic characteristics of very-high-rate GPS observations for seismology. Earth Planets Space 64(5):369–377. https://doi.org/10.5047/eps.2011.11.005

El-Mowafy A, Deo M, Kubo N (2017) Maintaining real-time precise point positioning during outages of orbit and clock corrections. GPS Solut 21:934–947. https://doi.org/10.1007/s10291-016-0583-4

Elsobeiey M, Al-Harbi S (2016) Performance of real-time precise point positioning using IGS real-time service. GPS Solut 20(3):565–571. https://doi.org/10.1007/s10291-015-0467-z

Fortunato M, Ravanelli M, Mazzoni A (2019) Real-time geophysical applications with android GNSS raw measurements. Remote Sens 11(18):1–13. https://doi.org/10.3390/rs11182113

Geng J, Bock Y, Melgar D, Crowell BW, Haase JS (2013) A new seismogeodetic approach applied to GPS and accelerometer observations of the 2012 Brawley seismic swarm: Implications for earthquake early warning. Geochemistry. Geophys Geosyst 14:2124–2142. https://doi.org/10.1002/ggge.20144

Geng T, Xie X, Fang R, Su X, Zhao Q, Liu G, Li H, Shi C, Liu J (2016) Real-time capture of seismic waves using high-rate multi-GNSS observations: application to the 2015 Mw 7.8 Nepal earthquake. Geophys Res Lett 43(1):161–167. https://doi.org/10.1002/2015GL067044

Hadas T, Bosy J (2015) IGS RTS precise orbits and clocks verification and quality degradation over time. GPS Solut 19(1):93–105. https://doi.org/10.1007/s10291-014-0369-5

Hung HK, Rau RJ, Benedetti E, Branzanti M, Mazzoni A, Colosimo G, Crespi M (2017) GPS seismology for a moderate magnitude earthquake: lessons learned from the analysis of the 31 October 2013 $M_L$ 6.4 Ruisui (Taiwan) earthquake. Ann Geophys 60(5):S0553. https://doi.org/10.4401/ag-7399

Kouba J (2015) A guide to using international GNSS service (IGS) products. https://kb.igs.org/hc/en-us/articles/201271873-A-Guide-to-Using-the-IGS-Products. Accessed 21 Feb 2022

Larson KM, Bodin P, Gomberg J (2003) Using 1-Hz GPS data to measure deformations caused by the Denali fault earthquake. Science 300(5624):1421–1424. https://doi.org/10.1126/science.1084531
Li X, Guo B, Lu C, Ge M, Wickert J, Schuh H (2014) Real-time GNSS seismology using a single receiver. Geophys J Int 198(1):72–89. https://doi.org/10.1093/gji/ggu113
Li X, Zheng K, Li X, Liu G, Ge M, Wickert J, Schuh H (2019) Real-time capturing of seismic waveforms using high-rate BDS, GPS and GLONASS observations: the 2017 Mw 6.5 Jiuzhaigou earthquake in China. GPS Solut 23(1):1–12. https://doi.org/10.1007/s10291-018-0808-9
Malys S, Jensen PA (1990) Geodetic point positioning with GPS carrier beat phase data from the CASA UNO experiment. Geophys Res Lett 17(5):651–654. https://doi.org/10.1029/GL017i005p00651
Melgar D, Melbourne TI, Crowell BW, Geng J, Szeliga W, Scrivner C, Santillan M, Goldberg DE (2020) Real-time high-rate GNSS displacements: performance demonstration during the 2019 Ridgecrest, California, earthquakes. Seismol Res Lett 91(4):1943–1951. https://doi.org/10.1785/0220190223
Nie Z, Gao Y, Wang Z, Ji S, Yang H (2018) An approach to GPS clock prediction for real-time PPP during outages of RTS stream. GPS Solut 22(1):1–14. https://doi.org/10.1007/s10291-017-0681-y
Nie Z, Liu F, Gao Y (2020) Real-time precise point positioning with a low-cost dual-frequency GNSS device. GPS Solut 24(1):1–11. https://doi.org/10.1007/s10291-019-0922-3
Shen N, Chen L, Liu J, Wang L, Tao T, Wu D, Chen R (2019) A review of global navigation satellite system (GNSS)-based dynamic monitoring technologies for structural health monitoring. Remote Sens 11(9):1001. https://doi.org/10.3390/rs11091001
Shu Y, Shi Y, Xu P, Niu X, Liu J (2017) Error analysis of high-rate GNSS precise point positioning for seismic wave measurement. Adv Sp Res 59(11):2691–2713. https://doi.org/10.1016/j.asr.2017.02.006
Shu Y, Fang R, Li M, Shi C, Li M, Liu J (2018a) Very high-rate GPS for measuring dynamic seismic displacements without aliasing: performance evaluation of the variometric approach. GPS Solut 22(4):1–13. https://doi.org/10.1007/s10291-018-0785-z
Shu Y, Fang R, Geng J, Zhao Q, Liu J (2018b) Broadband velocities and displacements from integrated GPS and accelerometer data for high-rate seismogeodesy. Geophys Res Lett 45(17):8939–8948. https://doi.org/10.1029/2018GL079425
Takasu T, Yasuda A (2009) Development of the low-cost RTK-GPS receiver with an open source program package RTKLIB. In: Int Symp GPS/GNSS (January 2009):4–6
Tang X, Roberts GW, Li X, Hancock CM (2017) Real-time kinematic PPP GPS for structure monitoring applied on the Severn suspension bridge. UK Adv Sp Res 60(5):925–937. https://doi.org/10.1016/j.asr.2017.05.010
Tu R, Liu J, Lu C, Zhang R, Zhang P, Lu X (2017) Cooperating the BDS, GPS, GLONASS and strong-motion observations for real-time deformation monitoring. Geophys J Int 209(3):1408–1417. https://doi.org/10.1093/gji/ggx099
Wang J, Meng X, Qin C, Yi J (2016) Vibration frequencies extraction of the forth road bridge using high sampling GPS data. Shock Vib 2016:1–18. https://doi.org/10.1155/2016/9807861
Wang Z, Li Z, Wang L, Wang X, Yuan H (2018) Assessment of multiple GNSS real-time SSR products from different analysis centers. ISPRS Int J Geo Inform. https://doi.org/10.3390/ijgi7030085
Wang L, Li Z, Ge M, Neitzel F, Wang X, Yuan H (2019) Investigation of the performance of real-time BDS-only precise point positioning using the IGS real-time service. GPS Solut 23(3):1–12. https://doi.org/10.1007/s10291-019-0856-9
Xu P, Du F, Shu Y, Zhang H, Shi Y (2021) Regularized reconstruction of peak ground velocity and acceleration from very high-rate GNSS precise point positioning with applications to the 2013 Lushan $M_w$6.6 earthquake. J Geod 95(1):1–22. https://doi.org/10.1007/s00190-020-01449-6
Yigit CO, El-Mowafy A, Bezcioglu M, Dindar AA (2020) Investigating the effects of ultra-rapid, rapid vs. Final precise orbit and clock products on high-rate GNSS-PPP for capturing dynamic displacements. Struct Eng Mech 73(4):424–436. https://doi.org/10.12989/sem.2020.73.4.427
Yigit CO, El-Mowafy A, Anil Dindar A, Bezcioglu M, Tiryakioglu I (2021) Investigating performance of high-rate GNSS-PPP and PPP-AR for structural health monitoring: dynamic tests on shake table. J Surv Eng 147(1):05020011. https://doi.org/10.1061/(asce)su.1943-5428.0000343
Zheng K, Zhang X, Li X, Li P, Sang J, Ma T, Schuh H (2019) Capturing co-seismic displacement in real time with mixed single- and dual-frequency receivers: application to the 2018 $M_w$7.9 Alaska earthquake. GPS Solut 23(1):1–14. https://doi.org/10.1007/s10291-018-0794-y



**Mert Bezcioglu** obtained his Ph.D. from Gebze Technical University in 2022 and is a research assistant in the Geomatics Engineering Department at Gebze Technical University. His current research interest is high-rate GNSS applications.

**Cemal Ozer Yigit** is a professor in Geomatics Engineering at Gebze Technical University, Turkey. His research areas include structural health monitoring, crustal deformation monitoring, natural hazard early warning, deformation analysis, high-rate GNSS applications.

**Baris Karadeniz** is a research assistant and graduate student in the Geomatics Engineering Department at Gebze Technical University. His research interest is high-rate GNSS-PPP, structural health monitoring and deformation monitoring.

**Ahmet Anil Dindar** received a Ph.D. from Boğaziçi University in 2009 and is an assistant professor at Gebze Technical University Department of Civil Engineering. His research areas are the performance-based design of RC structures and structural health monitoring.

**Ahmed El-Mowafy** is a Professor and the Director of Graduate Research of the School of Earth and Planetary Sciences at Curtin University Australia. His research areas include precise positioning and navigation using GNSS, integrity monitoring, structure deformation monitoring, POD, and estimation theory. He is the chair of the IAG working group on Integrity Monitoring for Precise Positioning, sets on the Editorial Board of five journals, and published more than 200 research papers.

**Özgür Avcı** is NRS&Monitoring department manager at SistemAS Company. He graduated from Istanbul Technical University Geodesy and Photogrammetry Department and obtained his MSc. in Geodesy engineering from Bogazici University Kandilli Observatory in 2007. He is working on using GNSS in multidisciplinary monitoring projects.